Journal of Solid State Chemistry 182 (2009) 364–373

Contents lists available at ScienceDirect

Journal of Solid State Chemistry

journal homepage: www.elsevier.com/locate/jssc

Metallic Re–Re bond formation in different MRe$_2$O$_6$ (M = Fe, Co, Ni) rutile-like polymorphs: The role of temperature in high-pressure synthesis

D. Mikhailova [a,b,*], H. Ehrenberg [b], S. Oswald [b], D. Trots [c], G. Brey [d], H. Fuess [a]

[a] Institute for Materials Science, Darmstadt University for Technology, D-64287 Darmstadt, Germany
[b] Institute for Complex Materials, IFW Dresden, P. O. BOX 270116, D-01171, Dresden, Germany
[c] Hamburger Synchrotronstrahlungslabor, Notkestr. 85, D-22603 Hamburg, Germany
[d] Institute for Geosciences, Johann Wolfgang Goethe-University Frankfurt am Main, Altenhöferallee 1, D-60438 Frankfurt am Main, Germany

ARTICLE INFO

Article history:
Received 22 August 2008
Received in revised form
21 October 2008
Accepted 3 November 2008
Available online 13 November 2008

Keywords:
3*d*-metal rhenium oxide MRe$_2$O$_6$
Rutile-like structure
Polymorphism
High-pressure synthesis
Re–Re bond
Magnetism
XPS spectra

ABSTRACT

Different polymorphs of MRe$_2$O$_6$ (M = Fe, Co, Ni) with rutile-like structures were prepared using high-pressure high-temperature synthesis. For syntheses temperatures higher than ~1573 K, tetragonal rutile-type structures ($P4_2/mnm$) with a statistical distribution of M- and Re-atoms on the metal position in the structure were observed for all three compounds, whereas rutile-like structures with orthorhombic or monoclinic symmetry, partially ordered M- and Re-ions on different sites and metallic Re–Re-bonds within Re$_2$O$_{10}$-pairs were found for CoRe$_2$O$_6$ and NiRe$_2$O$_6$ at a synthesis temperature of 1473 K. According to the XPS measurements, a mixture of Re^{+4}/Re^{+6} and M^{2+}/M^{3+} is present in both structural modifications of CoRe$_2$O$_6$ and NiRe$_2$O$_6$. The low-temperature forms contain more Re^{+4} and M^{3+} than the high-temperature forms. Tetragonal and monoclinic modifications of NiRe$_2$O$_6$ order with a ferromagnetic component at ~24 K, whereas tetragonal and orthorhombic CoRe$_2$O$_6$ show two magnetic transitions: below ~17.5 and 27 K for the tetragonal and below 18 and 67 K for the orthorhombic phase. Tetragonal FeRe$_2$O$_6$ is antiferromagnetic below 123 K.

1. Introduction

Phase relationships and crystal structures of existing compounds in the system Mo–Re–O [1,2] and V–Re–O [3] were intensively investigated due to their potential catalytical activity. In the quasibinary ReO$_2$–MoO$_2$-system a Mo$_x$Re$_{1-x}$O$_2$ solid solution with the orthorhombic ReO$_2$-structure and metallic M–M-bond is stable for $0 \leqslant x \leqslant 0.35$ at 1173–1473 K, whereas a two-phase region consisting of orthorhombic Mo$_x$Re$_{1-x}$O$_2$ and monoclinic MoO$_2$ was found for $0.35 < x \leqslant 1$ [1]. For V$_x$Re$_{1-x}$O$_2$, the monoclinic MoO$_2$-type structure was registered for $x \geqslant 0.98$ and the rutile structure was detected for $0.98 < x \leqslant 0.85$ [3]. The increasing Re-content in the phase decreases linearly the insulator–metal transition temperature and at the same time increases the molar magnetic susceptibility. The rutile structure was also stabilized for V$_{0.5}$Re$_{0.5}$O$_2$ by high-pressure high-temperature (HPHT) synthesis [4].

The study of M_xRe$_{1-x}$O$_2$ for M-3*d* transition metals is limited to only a few works [5–8]. The best known compounds crystallize either in the rutile-structure with a random distribution of cations or rutile-like structures with or without cation ordering. MnReO$_4$ (Mn$_{0.5}$Re$_{0.5}$O$_2$) [5,7] and ZnReO$_4$ (Zn$_{0.5}$Re$_{0.5}$O$_2$) [5] adopt a wolframite-type structure without any metallic bond. Sc^{3+} demonstrates similarity with heavy rare earth elements in Re-containing compounds forming Sc$_6$ReO$_{12}$ with fluorite-like structure [9], and with 3*d*-elements forming ScRe$_2$O$_6$ with a new rutile-derivated monoclinic structure containing Re$_2$O$_{10}$-units with Re–Re bonds [8]. Compounds MReO$_4$ for M = Fe, Co, Ni were obtained for the first time by Sleight [5] using HPHT. FeReO$_4$ crystallizes in the tetragonal rutile-structure with a random cation occupation, whereas an increasing Fe-content in the compound causes an ordering of the cations resulting in the formation of a superstructure: a tri-α-PbO$_2$-type was proposed for Fe$_2$ReO$_6$. For CoReO$_4$ a new rutile-derivated type with an ordering of two cations was postulated [6], the structure of NiReO$_4$ is not solved yet [5]. Despite the lack of physical properties investigations of rutile-like Re- and 3*d*-containing complex oxides some of them seem to demonstrate metallic type of conductivity due to the delocalization of d electrons of Re-cations on Re–O–Re–O and Re–Re–Re linkages. For example, the decreasing of electrical resistivity on cooling was measured for FeReO$_4$, MnReO$_4$ [5] and

* Corresponding author at: Institute for Materials Science, Darmstadt University for Technology, D-64287 Darmstadt, Germany. Tel.: +49 6151 162894; fax: +49 6151 166023.
E-mail address: d.mikhailova@ifw-dresden.de (D. Mikhailova).

0022-4596/$ - see front matter © 2008 Elsevier Inc. All rights reserved.
doi:10.1016/j.jssc.2008.11.001

$ScRe_2O_6$ [8]. At the same time, there are strong magnetic interactions in 3*d*/Re-containing oxides leading to a high temperature of magnetic ordering: T_N of 210 K for $FeReO_4$ [5], T_N of 275 K and T_c of 225 K for $MnReO_4$ [7], and T_c above room temperature was measured for $ScRe_2O_6$ [8]. In the latter case only Re-ions (and itinerant electrons) are contributing to the magnetic moments.

The preparation by HPHT syntheses, crystal structures and magnetic properties of $FeRe_2O_6$, $CoRe_2O_6$ and $NiRe_2O_6$ are reported. $FeRe_2O_6$ crystallizes in the tetragonal rutile-type with Fe and Re sharing one crystallographic site. Two more polymorphs have been observed for each of the other compounds $CoRe_2O_6$ and $NiRe_2O_6$, controlled by the temperature of synthesis.

2. Experimental

Synthesis: A high-pressure high-temperature (HPHT) synthesis of MRe_2O_6 (M = Fe, Co, Ni) was performed in a Girdle-Belt apparatus with pyrophyllite as the pressure-transmitting medium. A graphite furnace with a platinum capsule inside containing the reactants was used for the experiment. Mixtures of MO (Alfa Aesar, 99.99%), ReO_3 (Strem Chemicals, 99.9%) and Re (Strem Chemicals, 99.99%) were ground in an agate mortar under acetone and filled in a platinum capsule. The sample holder was pressed up to 5 GPa before the temperature was raised to 1473 or 1573 K with a rate of 50 K/min. The heating current was switched off after 120 min, and after cooling to room temperature, pressure was released.

X-ray powder diffraction (*XRD*): Phase analysis and determination of cell parameters at room temperature were carried out using X-ray powder diffraction with a STOE STADI P diffractometer (Mo-$K\alpha_1$-radiation, $\lambda = 0.7093$ Å) in steps of 0.02° for 2 Theta from 3° to 45° in transmission mode for flat samples.

Crystal structure determination: The crystal structures of MRe_2O_6, M = Fe, Co, Ni, were solved by single-crystal X-ray diffraction using the Xcalibur system from Oxford Diffraction. The software packages SHELXS [10] and SHELXL [11] were used for structure solution and refinement as included in X-STEP32 [12].

High-temperature structure investigations: High-temperature structure investigations in the temperature range of 295–1173 K on MRe_2O_6 powders have been performed by synchrotron diffraction at beamline B2 [13] of the Hamburger Synchrotronstrahlungslabor at DESY (Hamburg, Germany) with the on-site readable image-plate detector OBI [14] and a STOE furnace, equipped with a EUROTHERM temperature controller and a capillary spinner. The wavelength of 0.49962(1) Å was determined from the positions of 8 reflections from a LaB_6 reference material. After heating up to 1173 K and subsequent cooling, the MRe_2O_6 samples were analyzed at room temperature again to check the reversibility of temperature induced changes. All diffraction patterns have been analyzed by using the software package WinPLOTR [15]. Only isotropic thermal displacement parameters have been refined by the Rietveld method.

Thermoanalysis: A simultaneous thermal analyzer NETZSCH STA 429 (CD) operated with dry and purified Ar was used to register mass loss and thermal flux curves. About 30 mg of MRe_2O_6 were heated in an Al_2O_3-crucible in Ar-atmosphere with a rate of 5°/min from 20 up to 1150 °C.

X-ray photoelectron spectroscopy (*XPS*) *measurements*: The X-ray photoelectron spectroscopic measurements were carried out at a PHI 5600 CI system using an Al $K\alpha$ 350 W monochromatized X-ray source and a hemispherical analyzer at a pass energy of 29 eV. When necessary, surface charging was minimized by means of a low-energy electron flood gun. The system base pressure was about 10^{-9} mbar. ReO_3 (Strem Chemicals, 99.9%), Co_3O_4 (Alfa Aesar, 99.99%) and NiO (Alfa Aesar, 99.99%) powders were used as reference materials for the estimation of the valence states of Co, Ni and Re ions in the ternary phases. The binding energy scale was calibrated from the carbon contamination using the C 1s peak at 285.0 eV.

Magnetization measurements: The magnetic properties of MRe_2O_6 (M = Fe, Co, Ni) have been studied with a superconducting quantum interference device (SQUID) from Quantum Design. Measurements were performed upon heating in field-cooled (FC) and zero-field cooled (ZFC) mode in the temperature range from 1.7 to 350 K and with applied field strengths up to 6.5 T.

3. Results and discussion

3.1. Synthesis and sample characterisation

Depending on the synthesis temperature different structural modifications were obtained for $NiRe_2O_6$ and $CoRe_2O_6$ at the constant external pressure: phases with the tetragonal rutile-structure are formed at 1573 K, whereas monoclinic rutile-derivated structures were obtained from synthesis at 1473 K ("low-temperature modifications"). $FeRe_2O_6$ was prepared at 1573 K only. Diffraction patterns of low-temperature modifications were similar to the one of high-pressure form of VO_2 [16]. The conditions of synthesis and the lattice parameters are listed in Table 1. XRD patterns of tetragonal $FeRe_2O_6$ and of the low-temperature modifications of $CoRe_2O_6$ and $NiRe_2O_6$ are presented in Fig. 1.

According to thermoanalyses mass losses were observed for tetragonal $CoRe_2O_6$ and $NiRe_2O_6$ in Ar-atmosphere above 1153 K, and CoO or NiO and Re(met.) were found as decomposition products after the high-temperature treatment during thermoanalyses.

3.2. Crystal structure

3.2.1. High-temperature modifications

According to single crystal structural data all high-temperature modifications of $FeRe_2O_6$, $CoRe_2O_6$ and $NiRe_2O_6$ crystallize in a tetragonal rutile-type structure (S.G. $P4_2/mnm$) with a random distribution of cations on the 2*a*-sites and without any metal–metal bonding (Table 2). Atomic positions and selected interatomic distances are presented in Table 3 and 4. The average (M,Re)–O–distance is nearly the same for all three compounds

Table 1
Synthesis conditions and lattice parameters of MRe_2O_6 (M = Fe, Co, Ni), calculated from powder diffraction data.

Compound	Synthesis conditions	Symmetry	Lattice parameters
$FeRe_2O_6$	5 GPa, 1573 K	Tetragonal	$a = 4.73954(8)$ Å, $c = 2.85881(5)$ Å, $Z = 2$
$CoRe_2O_6$	5 GPa, 1573 K	Tetragonal	$a = 4.7414(1)$ Å, $c = 2.84731(9)$ Å, $Z = 2$
$CoRe_2O_6$	5 GPa, 1473 K	Monoclinic	$a = 9.4176(2)$ Å, $b = 5.7161(1)$ Å, $c = 4.73808(9)$ Å, $\beta = 91.388(1)°$, $Z = 8$
$NiRe_2O_6$	5 GPa, 1573 K	Tetragonal	$a = 4.7313(1)$ Å, $c = 2.84552(8)$ Å, $Z = 2$
$NiRe_2O_6$	5 GPa, 1473 K	Monoclinic	$a = 9.3672(1)$ Å, $b = 5.72651(7)$ Å, $c = 4.72076(6)$ Å, $\beta = 91.7050(8)°$, $Z = 8$

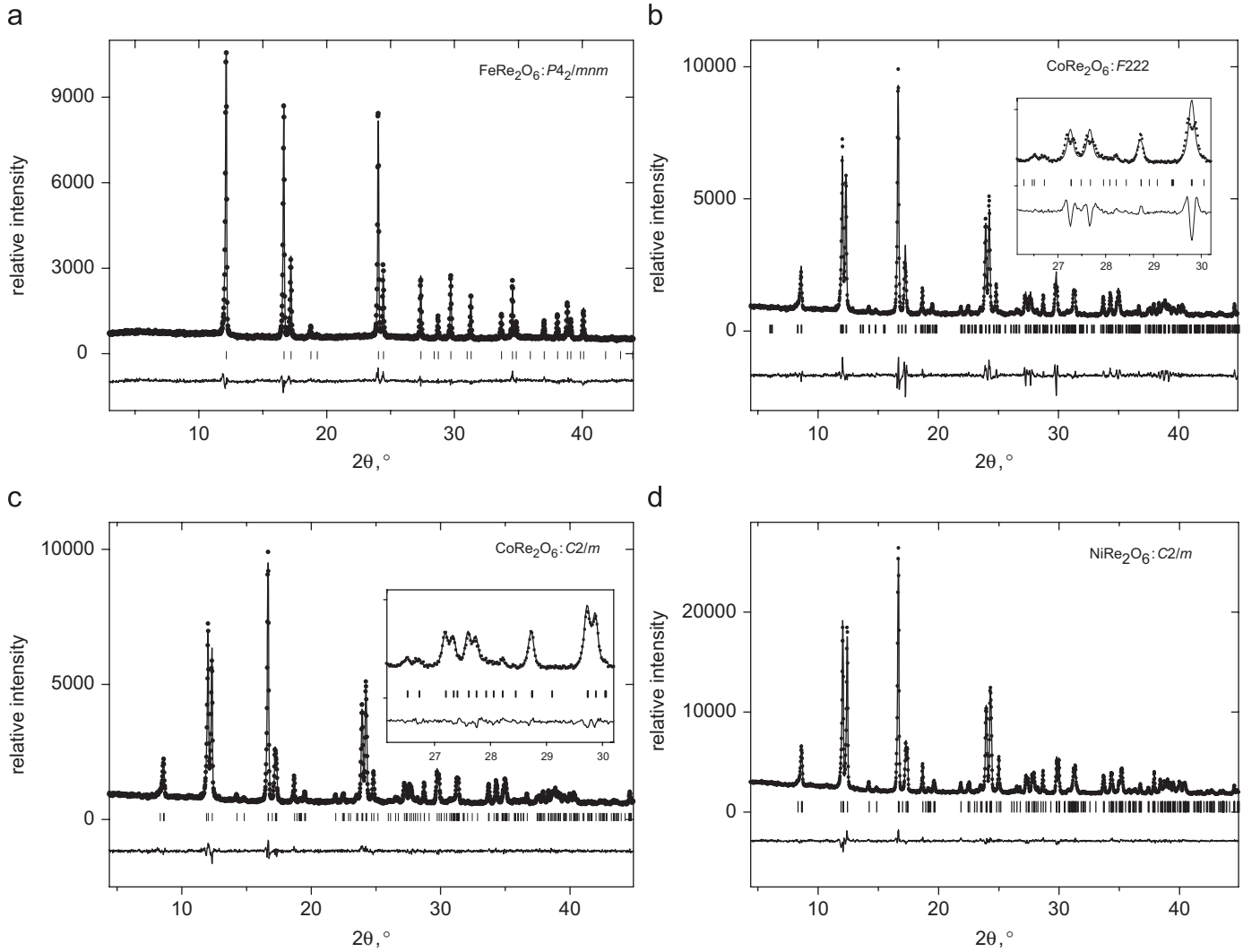

Fig. 1. (a) X-ray diffraction pattern of tetragonal $FeRe_2O_6$ (S.G. $P4_2/mnm$), observed and calculated profiles together with their difference curve. (b, c, d) X-ray diffraction patterns of the low-temperature modifications of $CoRe_2O_6$ and $NiRe_2O_6$. For $CoRe_2O_6$, two structural models using $F222$ (b) and $C2/m$ (c) space groups were refined based on the same data set (see text). The $NiRe_2O_6$ structure was refined in space group $C2/m$.

(1.98 Å). The tetragonal distortion of $(M,Re)O_6$-octahedra, calculated as the ratio $\zeta = d(M,Re\text{–}O)_{equatorial(4\ times)}/d(M,Re\text{–}O)_{apical(2\ times)}$ between averaged bond lengths in the equatorial plane and to apical oxygens, respectively, has the lowest value for $NiRe_2O_6$ ($\zeta = 1.008$) and the highest one for $CoRe_2O_6$ ($\zeta = 1.048$). Note that for TiO_6-octahedra in rutile TiO_2 a value $\zeta = 0.9827 < 1$ is calculated [17].

Sleight [5] has reported a tetragonal rutile-type modification (S.G. $P4_2/mnm$) in the system Fe–Re–O with the composition $FeReO_4$. The lattice parameters were: $a = 4.663$ Å, $c = 2.927$ Å. This means together with our results for $FeRe_2O_6$ the existence of a $Fe_xRe_{1-x}O_2$ solid solution for compositions at least within $0.33 \leqslant x \leqslant 0.50$. The "$a$" parameter of the unit cell becomes larger with increasing Re content in $Fe_xRe_{1-x}O_2$, whereas "c" decreases. The same effect was also found for $Cr_xRe_{1-x}O_2$ [18] and $Cr_xMo_{1-x}O_2$ [19] solid solutions.

In contrast to $Fe_xRe_{1-x}O_2$ no tetragonal solid solutions are found in the composition range $0.33 \leqslant x \leqslant 0.50$ for $Co_xRe_{1-x}O_2$ and $Ni_xRe_{1-x}O_2$. The composition $CoReO_4$ [6] adopts a rutile-like orthorhombic structure with an ordering of Co and Re on two distinct crystallographic sites and without Re–Re-bonds. Interatomic metal–oxygen distances Co–O and Re–O suppose rather the assignment of Co^{+3} and Re^{+5} than Co^{+2} and Re^{+6} [6]. $NiReO_4$, as reported in [5], adopts also a rutile-derivated structure, but no structural parameters were provided.

3.2.2. Low-temperature modifications

Low-temperature modifications of $NiRe_2O_6$ and $CoRe_2O_6$ crystallize in rutile-like structures with a partial ordering of cations. $NiRe_2O_6$ (Fig. 2, Table 1) adopts monoclinic symmetry, S.G. $C2/m$, as other oxides with similar structures, for example, $CrWO_4$ [20] and the high-pressure modification of VO_2 [16]. In this structure type two crystallographically non-equivalent $[(Ni,Re)O_4]_n$ and $[ReO_4]_n$ strings of edge-sharing ReO_6 and $(Ni,Re)O_6$ octahedra exist. The specific cation distribution on the metal sites is different in the structures of $NiRe_2O_6$ and $CrWO_4$: in $NiRe_2O_6$ the $4g$ site is exclusively occupied by Re atoms and the $4i$ site is occupied by Re and Ni, whereas in the $CrWO_4$ structure cation positions are completely ordered: Cr ions on the $4i$ and W ions on the $4g$ site. In both structures M_2O_{10} units with metallic M-M bonds exist between 5d cations (Fig. 3(b)). The Re–Re distance in the Re_2O_{10}-units is 2.611(2) Å and lower than in metallic Re (2.74 Å). The average Re–O distance is 1.95 Å and the

Table 2
Details of X-ray single-crystal data collection and structure refinement of polymorph modifications of MRe_2O_6 (M = Fe, Co, Ni).

Crystal data					
Chemical formula	$Fe_{1/3}Re_{2/3}O_2$	$Co_{1/3}Re_{2/3}O_2$	$Co_{1/3}Re_{2/3}O_2$	$Ni_{1/3}Re_{2/3}O_2$	$Ni_{1/3}Re_{2/3}O_2$
Formula weight	174.75	175.78	175.78	175.70	175.70
Crystal system	Tetragonal	Tetragonal	Orthorhombic	Tetragonal	Monoclinic
Space group	$P4_2/mnm$	$P4_2/mnm$	$F222$	$P4_2/mnm$	$C2/m$
Unit cell dimensions (Å and °)	$a = 4.741(4)$ $c = 2.865(7)$	$a = 4.728(1)$ $c = 2.847(1)$	$a = 13.531(3)$ $b = 13.192(2)$ $c = 5.7221(9)$	$a = 4.733(4)$ $c = 2.845(3)$	$a = 9.374(4)$ $b = 5.7225(14)$ $c = 4.7183(14)$ $\beta = 91.72(3)$
Cell volume (Å^3)	64.40(18)	63.64(4)	1021.4(3)	63.73(10)	252.99(15)
Z	2	2	32	2	8
Calculated density (g/cm^3)	9.014	9.173	9.145	9.156	9.226
Radiation type	Mo–$K\alpha$ ($\lambda = 0.71073$ Å)				
Temperature	299(2)	299(2)	299(2)	299(2)	299(2)
Crystal form, color	Prism, black	Prism, black	Prism, black	Prism, black	Prism, black
Crystal size (mm)	$0.010 \times 0.025 \times 0.040$	$0.030 \times 0.025 \times 0.020$	$0.06 \times 0.04 \times 0.03$	$0.020 \times 0.015 \times 0.015$	$0.025 \times 0.025 \times 0.015$
Data collection					
Diffractometer	Oxford Diffraction Xcalibur (TM); single-crystal X-ray diffractometer with sapphire CCD detector				
Data collection method	Rotation method data acquisition using ω and φ scans(s)				
Absorption coefficient (mm^{-1})	69.75	71.20	70.98	71.50	71.93
$F(000)$	224	134	2144	135	587
Theta range for data collection	6.08–27.38	6.10–27.22	3.01–27.92°	6.10–30.72	4.17–28.27
Range of h, k, l	$-5 \leqslant h \leqslant 6$, $-5 \leqslant k \leqslant 5$, $-2 \leqslant l \leqslant 3$	$-3 \leqslant h \leqslant 5$, $-5 \leqslant k \leqslant 6$, $-2 \leqslant l \leqslant 3$	$-16 \leqslant h \leqslant 17$, $-13 \leqslant k \leqslant 16$, $-7 \leqslant l \leqslant 7$	$-6 \leqslant h \leqslant 5$, $-5 \leqslant k \leqslant 6$, $-4 \leqslant l \leqslant 4$	$-12 \leqslant h \leqslant 11$, $-7 \leqslant k \leqslant 7$, $-6 \leqslant l \leqslant 6$
Reflections collected/unique	227/52 [R(int) = 0.0908]	174/51 [R(int) = 0.0644]	2168/560 [R(int) = 0.0974]	178/62 [R(int) = 0.0313]	992/312 [R(int) = 0.0354]
Completeness to Theta = 26.35°	98.1% (Theta = 27.38°)	98.1%	99.7%	92.5% (Theta = 30.72°)	97.2%
Refinement method	Full-matrix least-squares on F^2				
Data/restraints/parameters	52/0/9	51/0/9	560/0/39	62/0/9	312/0 /23
Goodness-of-fit on F^2	1.262	1.269	1.208	1.282	1.198
Final R indices [I > 2sigma(I)]	$R_1 = 0.0406$, $wR_2 = 0.0999$	$R_1 = 0.0369$, $wR_2 = 0.0808$	$R_1 = 0.0696$, $wR_2 = 0.2402$	$R_1 = 0.0213$, $wR_2 = 0.0450$	$R_1 = 0.0388$, $wR_2 = 0.0952$
R indices (all data)	$R_1 = 0.0448$, $wR_2 = 0.1015$	$R_1 = 0.0491$, $wR_2 = 0.0856$	$R_1 = 0.0782$, $wR_2 = 0.2538$	$R_1 = 0.0329$, $wR_2 = 0.0477$	$R_1 = 0.0432$, $wR_2 = 0.0977$
Extinction coefficient	0.46(11)	0.06(3)	0.0017(3)	0.006(5)	0.0021(5)
Largest diff. peak and hole	1.823 and −2.158 e/Å^3	1.623 and −1.382 e/Å^3	4.846 and −3.674 e/Å^3	0.999 and −1.192 e/Å^3	2.974 and −3.576 e/Å^3

average mixed (Re,Ni)–O distance 2.00 Å, which is somewhat shorter than in rhombohedral NiO with Ni^{2+} at room temperature [21]. All peaks on the powder diffraction pattern of the low-temperature $NiRe_2O_6$ are well described by this structure model (Fig. 1(d)). In contrast to the Ni-containing phase all investigated four single crystals of $CoRe_2O_6$ adopt orthorhombic symmetry (S.G. $F222$) with a larger unit cell, unambiguously revealed based on additional superstructure reflections. The same superstructure cell was also observed for another polymorph of $CrWO_4$ [22] (Fig. 3(a), Tables 1–3), but with a slightly different cation distribution: whereas W and Cr ions show a high degree of order on different sites (W atoms occupy 4a, 4b and 8h sites, Cr atoms 8i and 8j), the distribution of Co and Re is disordered (Table 2). The Re–Re bonds (2.539 Å) are due to Re-ions on the 8h-site as the W–W-bonds in orthorhombic $CrWO_4$. The Re–Re distance in the low temperature polymorph is shorter for the Co- than for the Ni-compound, indicating that more electrons of Re, which are not involved in Re–O bonds, participate in the metallic Re–Re bonds. The orthorhombic unit cell of $CoRe_2O_6$ can be described as a superstructure of four monoclinic cells of $NiRe_2O_6$, in which each second $[ReO_4]_n$ chain of edge sharing ReO_6 octahedra is broken by $(Co,Re)O_6$ octahedra, so that a sequence of octahedra $[ReO_6]$–$[(Co,Re)O_6]$–$[ReO_6]$–⋯ appears instead of $[ReO_6]$–$[ReO_6]$–$[ReO_6]$–⋯. Accordingly, both the monoclinic and the orthorhombic structure type are characterised by the formation of metallic Re–Re bonds in contrast to the high-temperature form. The monoclinic form is very sensitive to antiphase boundaries, where 3d-metal and Re-ions interchange site occupations, and the orthorhombic superstructure can be described as an ordered sequence of such antiphase boundaries. Therefore, several intermediate distributions of local Re–Re pairs are possible by some partial disorder in the specific site occupations, and the two polymorphs are just representing two different arrangements with a pronounced long-range order. Nevertheless, a high degree of residual disorder is reflected for both polymorphs by the mixed occupied sites. The formation of metallic Re–Re bonds seems to introduce a monoclinic distortion, which can be overcome by partial order in an orthorhombic superstructure as observed for all large single crystals. Note that the powder diffraction pattern of low-temperature $CoRe_2O_6$ cannot be satisfactorily explained based on the $F222$ space group (Fig. 1(d)), but only in $C2/m$, isotypic with $NiRe_2O_6$. For example, the (480) reflection at 27.68° in the $F222$ model (inset in the Fig. 1(b)) is clearly split into at least two reflections, well explained in the $C2/m$ model (inset in Fig. 1(c)). However, no monoclinic $CoRe_2O_6$ crystal with this structure model could be isolated for single crystal X-ray diffraction and are therefore probably limited to small domains, while large X-ray coherent crystals are only observed for a partially ordered superstructure.

The analysis of average interatomic (Re,M)–O distances in the low-temperature forms (for example, 1.93 and 2.01 Å for $CoRe_2O_6$) provide some information about the oxidation states of Co and Re:

Table 3
Atomic coordinates and anisotropic thermal displacement parameters ($Å^2$, $\times 10^3$) for MRe_2O_6.

Compound	S.G.	Atoms	Wyckoff site	x	y	z	Occupancy	U11	U22	U33	U23	U13	U12
$FeRe_2O_6$	$P4_2/mnm$	Fe	2a	0	0	0	0.33	7(1)	7(1)	31(2)	0	0	3(1)
		Re	2a	0	0	0	0.67	7(1)	7(1)	31(2)	0	0	3(1)
		O	4f	0.2931(15)	0.2931(15)	0	1	15(6)	15(6)	19(5)	0	0	7(4)
$CoRe_2O_6$	$P4_2/mnm$	Co	2a	0	0	0	0.33	6(2)	6(2)	22(2)	0	0	6(1)
		Re	2a	0	0	0	0.67	6(2)	6(2)	22(2)	0	0	6(1)
		O	4f	0.2870(30)	0.2870(30)	0	1	14(7)	14(7)	19(10)	0	0	−1(10)
$CoRe_2O_6$	F222	Re(1)	4a	0	0	0	1	20(2)	19(2)	53(6)	0	0	0
		Re(2)	8h	0.25	0.25	−0.0281(3)	1	13(1)	16(1)	10(1)	0	0	−6(1)
		Re(3)	4b	0	0	0.5	0.68(2)	1(2)	5(2)	17(3)	0	0	0
		Co(3)	4b	0	0	0.5	0.32(2)	1(2)	5(2)	17(3)	0	0	0
		Re(4)	8i	0.25	0.0044(2)	0.25	0.46(2)	32(2)	17(2)	28(2)	0	23(3)	0
		Co(4)	8i	0.25	0.0044(2)	0.25	0.54(2)	32(2)	17(2)	28(2)	0	23(3)	0
		Re(5)	8j	0.0082(2)	0.25	0.25	0.40(2)	12(2)	16(2)	22(2)	15(3)	0	0
		Co(5)	8j	0.0082(2)	0.25	0.25	0.60(2)	12(2)	16(2)	22(2)	15(3)	0	0
		O(1)	16k	0.1013(15)	0.0029(13)	0.251(7)	1	24(4)					
		O(2)	16k	0.250(2)	0.1069(18)	−0.008(4)	1	33(5)					
		O(3)	8f	0	0.143(2)	0	1	19(8)					
		O(4)	8f	0	0.361(3)	0	1	40(11)					
		O(5)	8j	0.155(2)	0.25	0.25	1	24(5)					
		O(6)	8j	−0.137(2)	0.25	0.25	1	26(6)					
$NiRe_2O_6$	$P4_2/mnm$	Ni	2a	0	0	0	0.33	11(1)	11(1)	22(1)	0	0	6(1)
		Re	2a	0	0	0	0.67	11(1)	11(1)	22(1)	0	0	6(1)
		O	4f	0.2938(17)	0.2938(17)	0	1	13(3)	13(3)	12(5)	0	0	4(4)
$NiRe_2O_6$	C2/m	Ni(1)	4i	0.2599(2)	0	0.4928(3)	0.68(2)	5(1)	8(1)	4(1)	0	0(1)	0
		Re(1)	4i	0.2599(2)	0	0.4928(3)	0.32(2)	5(1)	8(1)	4(1)	0	0(1)	0
		Re(2)	4g	0	0.7719(2)	0	1	7(1)	10(1)	6(1)	0	4(1)	0
		O(1)	8j	0.1437(12)	0.2420(18)	0.291(2)	1	9(2)					
		O(2)	4i	0.1099(17)	0	0.790(3)	1	8(3)					
		O(3)	4i	0.4066(17)	0	0.188(3)	1	8(3)					

For oxygen atoms in monoclinic $NiRe_2O_6$ and orthorhombic $CoRe_2O_6$ equivalent isotropic displacement parameters ($Å^2$ $\times 10^3$) were refined.

Table 4
Selected interatomic distances (Å) for the different polymorphs of MRe_2O_6.

Distances (Å) and angles (°)	$FeRe_2O_6$	$CoRe_2O_6$ (F222)	$CoRe_2O_6$ ($P4_2/mnm$)	$NiRe_2O_6$ (C2/m)	$NiRe_2O_6$ ($P4_2/mnm$)
Re(1)/M(1)–O(1)	1.965(10) (× 2)		1.92(2) (× 2)	1.99(1) (× 2)	1.967(11) (× 2)
Re(1)/M(1)–O(1)	1.994(7) (× 4)		2.01(2) (× 4)	2.00(1) (× 2)	1.982(8) (× 4)
M(Re)–M(Re)	2.865(7)		2.847(1)		2.845(3)
Re(1)–O(1)		1.99(3) (× 4)			
Re(1)–O(3)		1.89(3) (× 2)			
Re(1)–Re(3)		2.8610(5)			
Re(2)–O(2)		1.89(2) (× 2)		1.95(1) (× 2)	
Re(2)–O(6)		1.98(2) (× 2)			
Re(2)–O(5)		2.04(2) (× 2)			
Re(2)–Re(2)		2.539(4)		2.611(2)	
Re,Co(3)–O(4)		1.84(4) (× 2)			
Re,Co(3)–O(1)		1.98(3) (× 4)			
Re,Co(4)–O(1)		2.01(2) (× 2)			
Re,Co(4)–O(2)		2.00(2) (× 2)			
Re,Co(4)–O(2)		2.02(2) (× 2)			
Re,Co(5)–O(3)		2.01(2) (× 2)			
Re,Co(5)–O(4)		2.05(3) (× 2)			
Re,Co(5)–O(5)		1.97(3)			
Re,Co(5)–O(4)		1.99(3)			
Re,Ni(1)–O(2)				2.02(2)	
Re,Ni(1)–O(3)				2.02(2)	
Re(2)–O(1)				1.90(1) (× 2)	
Re(2)–O(3)				2.01(1) (× 2)	

The Co–O distance of 1.93 Å is too low for Co^{2+} (0.75 Å, high-spin) and O^{2-} (1.40 Å) and corresponds rather to the sum of ionic radii for Co^{3+} (0.55 Å, low-spin state) or Co^{3+} (0.61 Å, high-spin) and O^{2-}. The Re–O distance of 1.93 Å indicates Re^{5+} or Re^{6+}, whereas 2.01 Å would be expected for Re^{4+}–O. A similar assignment holds for $NiRe_2O_6$.

High-temperature structural investigations did not show any phase transitions below the phase decomposition temperatures.

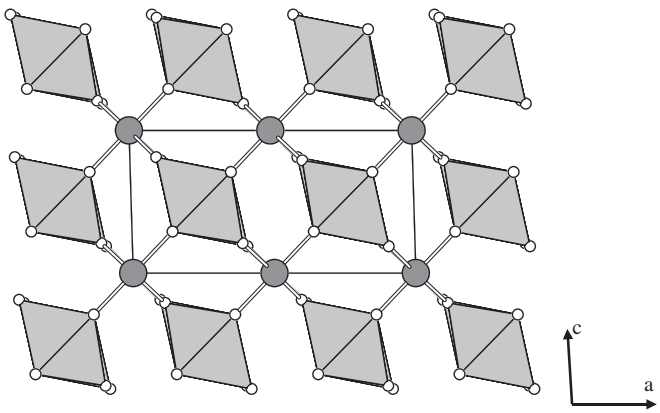

Fig. 2. Projection of monoclinic $NiRe_2O_6$ ($C2/m$) structure along [0–10]. Small white spheres are O^{2-} ions, large dark gray ones are Re ions (4g). In gray octahedra Re and Ni ions (4i) are statistically distributed.

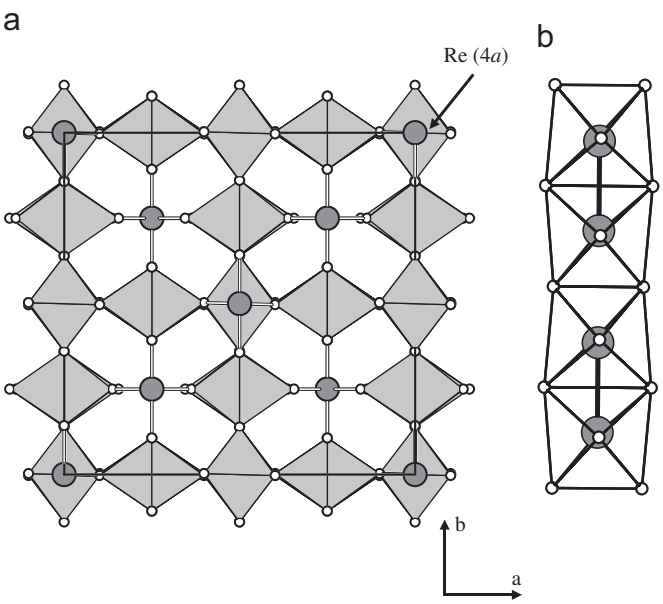

Fig. 3. (a) Projection of the orthorhombic $CoRe_2O_6$ ($F222$) structure along [001]. Small white spheres are O^{2-} ions, large dark gray ones are Re ions. gray octahedra are statistically occupied by Re and Co ions. (b) $[ReO_4]_n$ chains built up from ReO_6 edge-shared octahedra in the low-temperature modifications of $CoRe_2O_6$ and $NiRe_2O_6$. Re–Re bonds are represented by the thick black lines.

The average expansion coefficients along the "c" axes α_c for the tetragonal modifications of MRe_2O_6 are more than five times higher than those along the "a" axes α_a, for example $\alpha_c(NiRe_2O_6) = 1.31 \times 10^{-5}\,1/K$, $\alpha_a(NiRe_2O_6) = 2.53 \times 10^{-6}\,1/K$, or $\alpha_c(FeRe_2O_6) = 1.68 \times 10^{-5}\,1/K$, $\alpha_a(FeRe_2O_6) = 6.44 \times 10^{-7}\,1/K$. The thermal expansion of the low-temperature forms calculated for the same structural fragment as for the tetragonal ones is in the same order: $\alpha_{\text{"}c\text{"}}(CoRe_2O_6) = 1.34 \times 10^{-5}\,1/K$, $\alpha_{\text{"}a\text{"}}(CoRe_2O_6) = 3.05 \times 10^{-6}\,1/K$.

3.3. XPS measurements

The Re4$f_{7/2}$ and Re4$f_{5/2}$ XPS spectra of the orthorhombic, monoclinic and tetragonal modifications of MRe_2O_6 together with ReO_3 as a reference material are presented in Fig. 4. All spectra were calibrated with respect to the C1s peak. XPS spectra of Fe, Co and Ni are not shown, but have also been measured. It is known that the positions of the main Co2p photoemission peaks in ternary oxides do not change with an increase of the average oxidation state of Co from +2 to +3 or +4 as long as the oxygen coordination remains the same, while the position and the intensity of the satellite peaks dependent significantly on the metal oxidation state, see for example [23]. In our spectra there is a systematic shift of the Co2p and Ni2p cores towards higher binding energies, maybe as a result of a high positive charge of the sample due to photoelectron emission, so that the determination of the positions of the satellites is not very reliable. It should be noted here explicitly that XPS represents the electronic structure of the surface region, influenced by contaminations or surface effects. For the bulk material the Re4$f_{7/2}$ core peak is more representative, because the kinetic energies of the detected and analyzed photoelectrons are about 700 eV for Co2p and 1440 eV for Re4$f_{7/2}$, allowing a photoelectron escape from about 1.5 times deeper regions for Re4$f_{7/2}$ than for Co2p and Ni2p. The shifts in binding energies between Re4$f_{7/2}$ and Re4$f_{5/2}$ peaks of Re^{+4} in ReO_2 and Re^{+6} in ReO_3 are significant [24]. The authors of [25] have established an exponential dependence of the binding energy on the oxidation state of Re in the compounds NH_4ReO_4, Re_2O_7, ReO_3, ReO_2 and metallic Re without consideration of the underlying structures. However, the difference in the positions of the Re4$f_{7/2}$ peaks for Re^{+7} in NH_4ReO_4 and Re_2O_7 points out an influence of the structural features on the XPS spectra: in ammonium perrhenate only corner-sharing ReO_4-tetrahedra exist, in contrast to both corner-sharing ReO_4-tetrahedra and ReO_6-octahedra in Re_2O_7. Our measurements on ReO_3 (Fig. 4a) reveal the Re4$f_{7/2}$ peak of ReO_2 at 43.6 eV, which indicates the presence of Re^{+4} due to a partial reduction in the surface-near region. The broadening of Re peaks in MRe_2O_6 can also reflect Re in different oxidation states within one phase, but is also typically observed for strong-correlated electron systems. Each Re4f spectrum of MRe_2O_6 (M = Co, Ni) contains three peaks (Fig. 4c and a) which can be represented as a combination of Re^{+4} and Re^{+6}, although "Re^{+6}"-peaks are shifted to higher energies and "Re^{+4}"-peaks to lower energies. The relative area of the Re^{+4} peak is higher for the low-temperature modifications of the Co- and Ni-compound, while the area below the satellite peak of Re^{+6} is higher for the tetragonal modifications. This means, taking charge balance into account, the presence of higher concentrations of Co^{3+} and Ni^{3+} in the low-temperature modifications than in the tetragonal high-temperature forms[1]. The Re4f spectrum of $FeRe_2O_6$ (Fig. 4e) is more complex and exhibits an additional peak at 41.0 eV, which might indicate the presence of some metallic Re, although not observed in XRD.

From the XPS valence spectra of MRe_2O_6 (M = Fe, Co, Ni) one can expect a metallic behavior (Fig. 4f, d, b) of these compounds. The density of states at E_F is a little higher for orthorhombic $CoRe_2O_6$ than for tetragonal $CoRe_2O_6$ and significantly higher for monoclinic $NiRe_2O_6$ compared with tetragonal $NiRe_2O_6$. It correlates with the relative amount of Re ions in metallic Re–Re bonds: in the orthorhombic modification of $CoRe_2O_6$ only 37% of all Re atoms form metallic Re–Re bonds in contrast to 75% in the monoclinic form of $NiRe_2O_6$. The shape of MRe_2O_6 (M = Fe, Co, Ni) valence peaks is quite different from that of ReO_3 (Fig. 4f, d, b). According to a simplified model of the ReO_3 band structure without covalence contributions and based on a formal separation of the total electronic structure into an O2p and a Re5d band, the peak with ~2 eV-width just below the Fermi energy is interpreted as the Re5d-derived conduction band, and the major part of the p-band signal (between 3 and 10 eV) is also due to the Re-d

[1] Note that all experiments were performed at room temperature. "Low-temperature modification" and "high-temperature form" refers to the relative temperatures during syntheses.

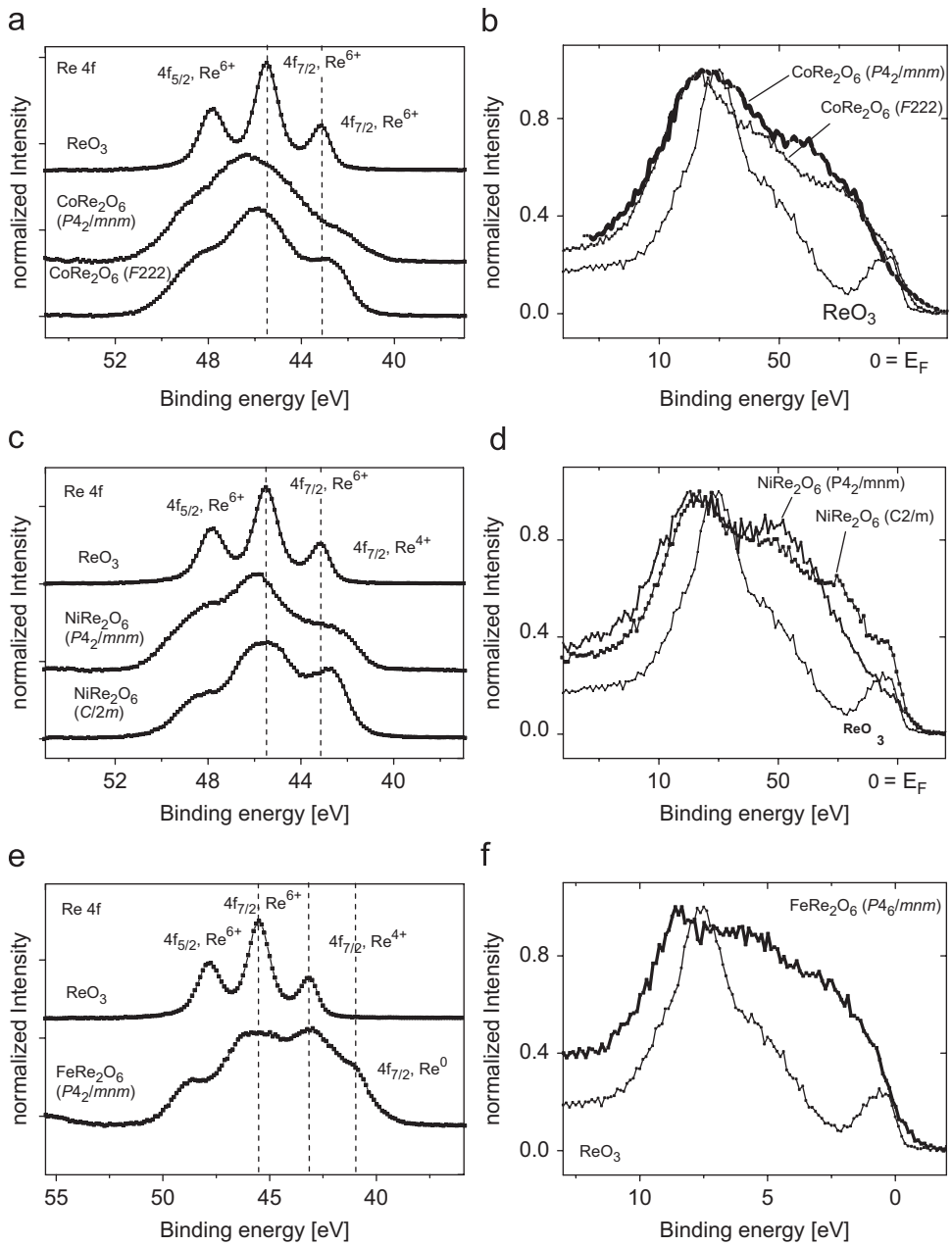

Fig. 4. (a) Re4$f_{7/2}$ and 4$f_{5/2}$ core peaks of ReO_3 and $CoRe_2O_6$ (orthorhombic and tetragonal modifications). (b) XPS valence spectra of orthorhombic and tetragonal $CoRe_2O_6$ and ReO_3. (c) Re4$f_{7/2}$ and 4$f_{5/2}$ core peaks of ReO_3 and $NiRe_2O_6$ (monoclinic and tetragonal modifications). (d) XPS valence spectra of monoclinic and tetragonal $NiRe_2O_6$ and ReO_3 as external standard. (e) Re4$f_{7/2}$ and 4$f_{5/2}$ core peaks of ReO_3 and tetragonal $FeRe_2O_6$.

component [26]. In our XPS spectra the 3*d* band of the *M* element must also be taken into consideration, which makes a more specific interpretation of the spectra without theoretical band structure calculations impossible.

3.4. Magnetic properties

The temperature dependences of the inverse specific susceptibility χ_m^{-1} of MRe_2O_6 (M = Fe, Co and Ni) are shown in Fig. 5. Tetragonal $FeRe_2O_6$ orders antiferromagnetically below $T = 123$ K in contrast to $FeReO_4$ [5] with a higher $T_N = 194$ K, in agreement with the higher concentration of Fe-ions in the latter compound. Tetragonal and monoclinic modifications of $NiRe_2O_6$ order with a ferromagnetic component at ~24 K, whereas both modifications of $CoRe_2O_6$ show two magnetic transitions at ~17.5 and 27 K for the tetragonal one and at 18 and 67 K for the orthorhombic phase. Field dependences of magnetization for tetragonal $CoRe_2O_6$ and $NiRe_2O_6$ are presented in Fig. 6. The coercivity field strength for the Co-compound is 50 G at 5 K. The pronounced differences between field-up and field-down branches at 5 K at higher field strengths (up to 6 T) is probably due to first-order field-induced transitions into the intermediate magnetic structure, which is stable between 17.5 and 27 K in zero-field. At 21 K, this magnetic structure exists already in zero-field, so that no such transition can be induced and no anomaly is observed in M(H) at this temperature. Magnetic moments μ_{eff}(exp) per formula unit $M_xRe_{1-x}O_2$ are calculated from the Curie constants in the paramagnetic region, obtained from fitting Eq. (1) to the observed data (Table 5).

$$M(T) = \frac{C}{T-\theta} + M_0 \quad (1)$$

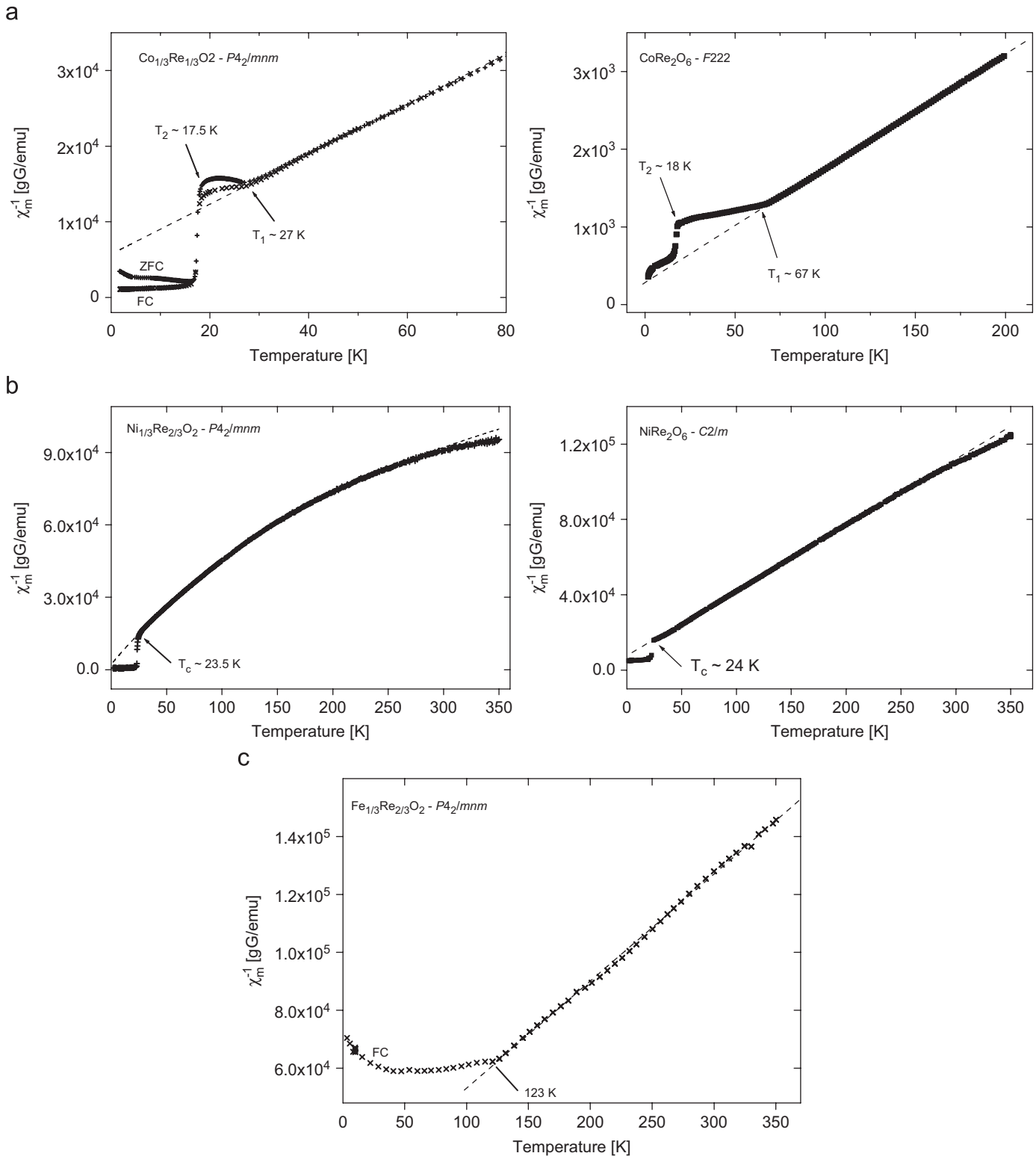

Fig. 5. (a) The temperature dependences of the inverse specific susceptibility χ_m^{-1} for the two modifications of $CoRe_2O_6$. (b) The temperature dependences of the inverse specific susceptibility χ_m^{-1} for the two modifications of $NiRe_2O_6$. (c) The temperature dependence of the inverse specific susceptibility χ_m^{-1} of tetragonal $FeRe_2O_6$.

Note that paramagnetic moments of the low-temperature forms of MRe_2O_6 are significantly higher than those for the tetragonal forms, which can be connected either with the more itinerant character of d electrons in the tetragonal forms or with a partial charge transfer from M to Re and therefore the formation of M-ions in a higher oxidation states. The theoretical effective magnetic moments per $M_{0.33}Re_{0.67}O_2$ unit, μ_{eff}(cal), were calculated from the spin only contributions of the 3d-ions, distinguished for the low-spin and high-spin states of M^{2+} and M^{3+}, respectively, according to the equation $\mu_{eff}(\text{cal}) = g[0.33S(S+1)]^{1/2}$, where g is the Landé splitting factor and S is the total spin. This simple model is based on delocalized Re electrons, supported by the XPS valence band measurements, which do not give a significant contribution to the paramagnetic

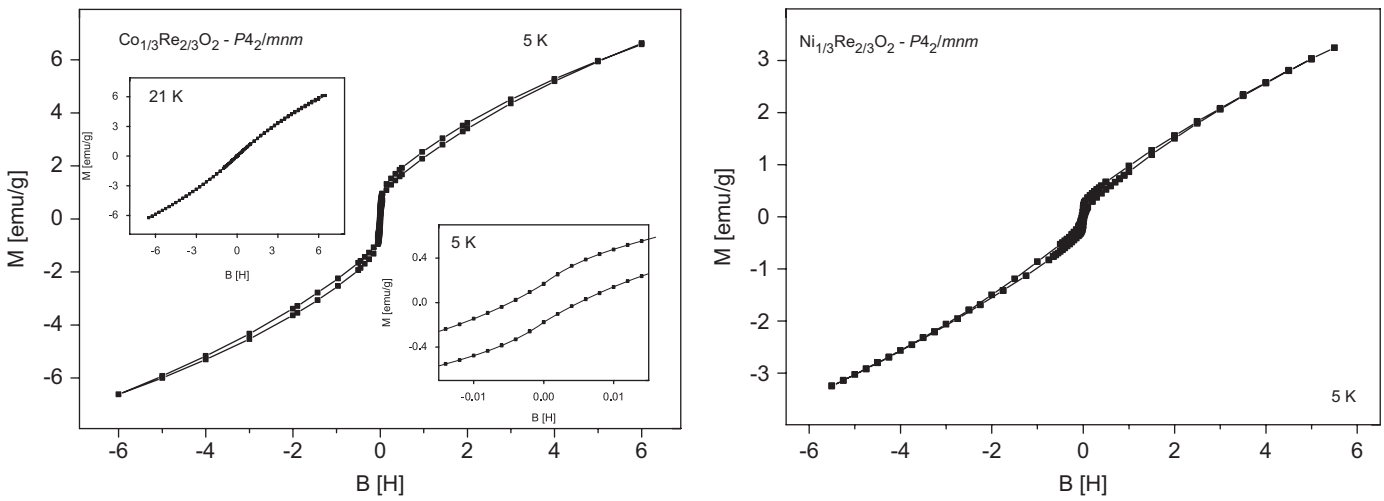

Fig. 6. Field dependence of magnetization for tetragonal $CoRe_2O_6$ and $NiRe_2O_6$.

Table 5
Magnetic properties of MRe_2O_6.

Compound	Space group	T_c (K)	$\chi_0 \times 10^6$ (Gg/emu)	Θ (K)	Temperature range for fit (K)	μ_{eff}(exp) (μ_B)
$CoRe_2O_6$	*F*222	67, 18	0	−18.9(2)	80–200	2.74(1)
$Co_{1/3}Re_{2/3}O_2$	$P4_2/mnm$	27, 17.5	0	−17.4(5)	25–350	2.06(1)
$NiRe_2O_6$	$C2/m$	24	0	−18.5(4)	50–300	2.00(1)
$Ni_{1/3}Re_{2/3}O_2$	$P4_2/mnm$	23.5	5.0(2)	−4.1(7)	30–350	1.59(2)
$Fe_{1/3}Re_{2/3}O_2$	$P4_2/mnm$	123 (T_N)	9.1(3)	−2.0(1.5)	160–300	3.06(3)

Magnetic moments are normalized to one formula unit $M_xRe_{1-x}O_2$. The standard deviations in brackets are determined as the limits, for which an up to 10% higher residual is obtained in the least-square fit than for the optimum fit for Eq. (1). χ_0 was calculated from M_0 in Eq. (1) as $\chi_0 = M_0/(M_x\,H)$.

Table 6
Spin-only calculated magnetic moments of $M_xRe_{1-x}O_2$ (M = Fe, Co,Ni) for low-spin and high-spin states of M.

Cation	Ground state term	Calculated magnetic moment per $M_{0.33}Re_{0.67}O_2$ (μ_B)	
		Low-spin configuration	High-spin configuration
Fe^{2+}, d^6	$^5D_4$	0.00	2.81
Fe^{3+}, d^5	$^6S_{5/2}$	1.00	3.40
Co^{2+}, d^7	$^4F_{9/2}$	1.00	2.22
Co^{3+}, d^6	$^5D_4$	0.00	2.81
Ni^{2+}, d^8	$^3F_4$	0.00	1.62
Ni^{3+}, d^7	$^4F_{9/2}$	1.00	2.22

moments. The same approximation was previously applied to similar systems, for example $Cr_xMo_{1-x}O_2$ [26]. From this point of view, the experimental paramagnetic moment of orthorhombic $CoRe_2O_6$ (2.74 μ_B) is in a good agreement with the calculated one for high-spin Co^{3+} (2.81 μ_B) and too high for high-spin Co^{2+} (2.22 μ_B) (Table 6). The measured paramagnetic moment of monoclinic $NiRe_2O_6$ (2.00 μ_B) is lower than the one calculated for high-spin Ni^{3+} (2.22 μ_B) and$^+$, but higher than the one for Ni^{2+} (1.62 μ_B), so that an intermediate electronic state of Ni between Ni^{2+} and Ni^{3+} with electron delocalization might be indicated. The lower magnetic moments in the tetragonal modifications of $CoRe_2O_6$ (2.06 μ_B) and $NiRe_2O_6$ (1.59 μ_B) may be due to the presence of some amount of high-spin M^{2+} in the compounds, which is indicated by the XPS measurements. The paramagnetic moment of Fe in the tetragonal modification corresponds to the oxidation state of Fe between +2 (high-spin) and +3 (high-spin).

4. Conclusion

Different modifications with rutile-derivated crystal structures of compounds with composition MRe_2O_6, M = Fe, Co and Ni, can be prepared, controlled by the temperature of synthesis. A random distribution of M and Re on one site results for higher temperatures. These compounds should be labelled as $(M_{1/3}Re_{2/3})O_2$ to distinguish them from the compounds MRe_2O_6 with a partial order of M and Re on distinct sites, obtained at lower temperatures. The symmetry of the crystal structures is reduced by this partial order and metallic Re-Re bonds are formed, accompanied by changes in the electronic configurations of the transition metals.

References

[1] Ö. Sävborg, Mater. Res. Bull. 11 (1976) 275–280.
[2] L.A. Klinikova, E.D. Skrebkova, Zh. Neorg. Khimii. 23 (1978) 180–183.
[3] Ö. Sävborg, M. Nygren, Phys. Stat. Sol. (A) 43 (1977) 645–652.
[4] K.G. Bramnik, H. Ehrenberg, R. Theissmann, H. Fuess, E. Morán, Z. Kristallogr. 218 (2003) 455–457.
[5] A.W. Sleight, J. Solid State Chem. 14 (1975) 597–598.
[6] W.H. Baur, W. Joswig, G. Pieper, D. Kassner, J. Solid State Chem. 99 (1992) 207–211.
[7] K.G. Bramnik, H. Ehrenberg, S. Buhre, H. Fuess, Acta Cryst. B 61 (2005) 246–249.
[8] D. Mikhailova, H. Ehrenberg, G. Miehe, D. Trots, C. Hess, R. Schneider, H. Fuess, J. Solid State Chem. 181 (2008) 190–198.
[9] D. Mikhailova, H. Ehrenberg, H. Fuess, J. Solid State Chem. 179 (2006) 3672–3680.
[10] G.M. Sheldrick, Acta Crystallogr. A 46 (1990) 467–473.
[11] G.M. Sheldrick, SHELXL97, Program for the Refinement of Crystal Structures, University of Göttingen, Germany, 1997.
[12] Stoe & Cie, X-STEP32, 2000, Stoe & Cie GmbH, Darmstadt, Germany.
[13] M. Knapp, C. Baehtz, H. Ehrenberg, H. Fuess, J. Synchrotron Radiat. 11 (2004) 328–334.

[14] M. Knapp, V. Joco, C. Baehtz, H.H. Brecht, A. Berghaeuser, H. Ehrenberg, H. von Seggern, H. Fuess, Nucl. Instrum. Methods A 521 (2004) 565–570.
[15] T. Roisnel, J. Rodriguez-Carvajal, Mater. Sci. Forum 378–381 (2001) 118–123.
[16] J. Galy, G. Miehe, Solid State Sci. 1 (1999) 433–448.
[17] T.M. Sabine, C.J. Howard, Acta Cryst. B 38 (1982) 701–702.
[18] D. Mikhailova, submitted to J. Solid State Chem.
[19] Y. Shimony, L. Ben-Dor, Mater. Res. Bull. 15 (1980) 227–232.
[20] M. Vlasse, J.-P. Doumerc, P. Peshev, J.-P. Chaminade, M. Pouchard, Rev. Chim. Min. 13 (1976) 451–458.
[21] G.A. Slack, J. Appl. Phys. 31 (1960) 1571–1582.
[22] Y. Shimony, L. Ben-Dor, Mater. Res. Bull. 18 (1983) 331–335.
[23] L. Dahéron, R. Dedryvère, H. Martinez, M. Ménetrier, C. Denage, C. Delmas, D. Conbeau, Chem. Mater. 20 (2008) 583–590.
[24] J.F. Moulder, W.F. Stickle, P.E. Sobol, K.D. Bomben, Handbook of X-ray Photoelectron Spectroscopy, Physical Electronics, Inc., 1995.
[25] A. Cimino, B.A. De Angelis, D. Gazzoli, M. Valigi, Z. Anorg. Allg. Chem. 460 (1980) 86–98.
[26] G.K. Wertheim, L.F. Mattheiss, M. Campagna, Phys. Rev. Lett. 32 (1974) 997–999.